

Metabolic alterations caused by the mutation and overexpression of the *Tmem135* gene

Wei-Hua Lee^{1,*}, Vijesh J Bhute^{2,*,#}, Hitoshi Higuchi¹ , Sakae Ikeda¹, Sean P Palecek² and Akihiro Ikeda¹ 

¹Department of Medical Genetics, University of Wisconsin-Madison, Madison, WI 53706, USA; ²Department of Chemical and Biological Engineering, University of Wisconsin-Madison, Madison, WI 53706, USA

Corresponding author: Akihiro Ikeda. Email: aikeda@wisc.edu

[#]Present address: Department of Chemical Engineering, Imperial College London, South Kensington, London, SW7 2AZ, UK

*These authors contributed equally to this paper.

Impact statement

Mitochondria are dynamic organelles undergoing fission and fusion. Proper regulation of this process is important for healthy aging process, as aberrant mitochondrial dynamics are associated with several age-related diseases/pathologies. However, it is not well understood how imbalanced mitochondrial dynamics may lead to those diseases and pathologies. Here, we aimed to determine metabolic alterations in tissues and cells from mouse models with over-fused (fusion > fission) and over-fragmented (fusion < fission) mitochondria that display age-related disease pathologies. Our results indicated tissue-dependent sensitivity to these mitochondrial changes, and metabolic pathways likely affected by aberrant mitochondrial dynamics. This study provides new insights into how dysregulated mitochondrial dynamics could lead to functional abnormalities of tissues and cells.

Abstract

Mitochondria are dynamic organelles that undergo fission and fusion. While they are essential for cellular metabolism, the effect of dysregulated mitochondrial dynamics on cellular metabolism is not fully understood. We previously found that transmembrane protein 135 (*Tmem135*) plays a role in the regulation of mitochondrial dynamics in mice. Mice homozygous for a *Tmem135* mutation (*Tmem135*^{FUN025/FUN025}) display accelerated aging and age-related disease pathologies in the retina including the retinal pigment epithelium (RPE). We also generated a transgenic mouse line globally overexpressing the *Tmem135* gene (*Tmem135* TG). In several tissues and cells that we studied such as the retina, heart, and fibroblast cells, we observed that the *Tmem135* mutation causes elongated mitochondria, while overexpression of *Tmem135* results in fragmented mitochondria. To investigate how abnormal mitochondrial dynamics affect metabolic signatures of tissues and cells, we identified metabolic changes in primary RPE cell cultures as well as heart, cerebellum, and hippocampus isolated from *Tmem135*^{FUN025/FUN025} mice (fusion > fission) and *Tmem135* TG mice (fusion < fission) using nuclear magnetic resonance spectroscopy. Metabolomics analysis revealed a tissue-dependent response to *Tmem135* alterations, whereby significant metabolic changes were observed in the heart of both *Tmem135* mutant and TG mice as

compared to wild-type, while negligible effects were observed in the cerebellum and hippocampus. We also observed changes in *Tmem135*^{FUN025/FUN025} and *Tmem135* TG RPE cells associated with osmosis and glucose and phospholipid metabolism. We observed depletion of NAD⁺ in both *Tmem135*^{FUN025/FUN025} and *Tmem135* TG RPE cells, indicating that imbalance in mitochondrial dynamics to both directions lowers the cellular NAD⁺ level. Metabolic changes identified in this study might be associated with imbalanced mitochondrial dynamics in heart tissue and RPE cells which can likely lead to functional abnormalities.

Keywords: Mitochondrial dynamics, *Tmem135*, mouse models, metabolomics, retinal pigment epithelium, heart

Experimental Biology and Medicine 2020; 245: 1571–1583. DOI: 10.1177/1535370220932856

Introduction

Mitochondria are dynamic organelles that undergo fusion, fission, and degradation. Mitochondrial fusion in mammals is mediated by dynamin-related GTPases, mitofusin 1 and 2

(MFN1 and MFN2), that are responsible for fusion of mitochondrial outer membranes,¹ and optic atrophy 1 (OPA1), also a dynamin-related GTPase, that facilitates fusion of mitochondrial inner membranes.² Mitochondrial fission in mammals is mediated by dynamin-related protein 1 (DRP1,

or dynamin 1-like [DNM1L]), which is also a large GTPase that can be recruited to the mitochondrial outer membrane to constrict mitochondria resulting in their division.³ Changes in mitochondrial dynamics have been associated with aging and altered lifespan in yeast,⁴ *Caenorhabditis elegans*,⁵ and *Drosophila*.⁶ Mutations in mitochondrial fusion and fission proteins have also been associated with human diseases including peripheral neuropathies, optic atrophy, encephalopathy, and encephalomyopathy.^{7–12} The consequences of abnormal mitochondrial dynamics in the heart have been extensively studied by targeting regulators of mitochondrial dynamics in mice. Mice with *Drp1* depletion in the adult heart (causing over-fused mitochondria) show dilated cardiomyopathy, while mice with ablation of both *Mfn1* and *Mfn2* in the adult heart (causing decreased mitochondrial fusion) display cardiac hypertrophy.¹³ Imbalanced processing of OPA1 (causing fragmentation of mitochondria) in mice results in dilated cardiomyopathy.¹⁴ These results highlight the importance of balanced mitochondrial dynamics for normal structures and functions of the heart. While mitochondria are essential for cellular metabolism¹⁵ and mitochondrial disorders represent common forms of genetic metabolic diseases in human,^{16,17} it is still not fully understood how mitochondrial dynamics affect cellular metabolism.

Transmembrane 135 (TMEM135) was originally suggested to be involved in fat storage, resistance for cold stress, and longevity in *C. elegans*.¹⁸ We previously identified a mouse gene, *Tmem135*, and discovered its role in regulating mitochondrial dynamics.¹⁹ Mice homozygous for a *Tmem135* mutation (*Tmem135*^{FUN025/FUN025}) show phenotypes associated with accelerated aging in the retina including a significant photoreceptor cell degeneration, increase of ectopic photoreceptor synapses, and upregulation of a retinal stress marker, glial fibrillary acidic protein, as well as age-related pathologies in the retina including increased autofluorescence and active microglia in the outer retina, thickening of the retinal pigment epithelium (RPE) and reduced retinal functions measured by electroretinograms.¹⁹ Mitochondria were enlarged and the mitochondrial network appeared to be more fused in fibroblasts and RPE cells isolated from *Tmem135*^{FUN025/FUN025} mice, and in inner segments of photoreceptor cells in the *Tmem135*^{FUN025/FUN025} retina.¹⁹ Conversely, transgenic mice globally overexpressing wild-type (WT) *Tmem135* (*Tmem135* TG) display a fragmented mitochondrial network in fibroblasts and RPE cells, as well as the heart muscle.^{19,20} Pathologically, the heart of *Tmem135* TG mice shows collagen accumulation and hypertrophy.²⁰ We also found that gene expression profiles of the *Tmem135* TG heart share common features with the aged heart.²⁰ These mouse models provide unique opportunities to examine the effect of dysregulated mitochondrial dynamics on the integrity and metabolism of their tissues.

Here, in order to investigate how abnormal mitochondrial dynamics affect metabolic signatures of tissues and cells, we examined metabolic changes associated with mutation and overexpression of the *Tmem135* gene in the heart and brain tissues (hippocampus and cerebellum) as well as primary cultures of RPE cells. These tissues and

cells were selected based on their high energy demand, which may make them vulnerable to mitochondrial changes, as well as abnormal phenotypes observed in *Tmem135* mutant or TG mice.^{19,20} We observed that modulation of *Tmem135* activity leads to tissue-dependent effects. Specifically, we observed a high sensitivity of heart tissue to changes in *Tmem135* activity while some regions of the brain including cerebellum and hippocampus showed negligible effects. Additionally, we observed potential effects of increased oxidative stress in both *Tmem135* mutant and *Tmem135* TG models and also identified diverse metabolic alterations associated with each model in RPE cells. We also identified glutamine reduction to be a key aspect associated with *Tmem135* TG tissues and cells. Findings from this study will help us understand how mitochondrial dynamics affect metabolites and metabolic pathways in the heart tissue and RPE cells, which may indicate the mechanisms through which dysregulated mitochondrial dynamics lead to accelerating aging and disease phenotypes in *Tmem135* mouse models.

Materials and methods

Animals

All animal procedures were approved by the Animal Care and Use Committee at the University of Wisconsin-Madison. *Tmem135*^{FUN025/FUN025} mice were generated in the Northwestern University Center for Functional Genomics as previously described^{21,22} and were imported to and maintained at University of Wisconsin-Madison by crossing homozygous mutants to heterozygous mice.¹⁹ Genotyping for WT and *FUN025* alleles was performed as previously described.¹⁹ *Tmem135* TG mice were generated as previously described^{19,20} and maintained by breeding transgene-positive mice with transgene-negative siblings. Transgene-positive mice were detected by polymerase chain reaction using primers, m*Tmem135* F4 (GCAAGAGGAACCATCACGAC) and m*Tmem135* R6 (TGCCAAAACCCAGCCAC). C57BL/6J mice were obtained from The Jackson Laboratory and used as WT control mice for this study.

Tissue isolation

Three-month-old *Tmem135*^{FUN025/FUN025}, *Tmem135* TG, and WT (C57BL/6J) mice were euthanized by CO₂ inhalation. Heart and brain (cerebellum and hippocampus) tissues were quickly dissected out, rinsed in phosphate-buffered saline (PBS), snap frozen in liquid nitrogen, and stored at –80°C.

Cell culture

Primary RPE cultures were carried out as previously described²³ with a slight modification. Briefly, two-month-old mice (WT: C57BL/6J; *Tmem135* TG; *Tmem135*^{FUN025/FUN025}) were euthanized by CO₂ inhalation, and their eyes were removed and placed in ice-cold Dulbecco modified Eagle medium (DMEM; ATCC, Manassas, VA). Following the removal of the cornea, lens,

and retina under the microscope, the posterior eyecups were immersed in 0.25% (wt/vol) trypsin, 2.21 mM EDTA (CORNING, Manassas, VA) at 37°C for 1 h. RPE cells were dissociated from the Bruch's membrane by gentle aspiration and collected by centrifuging for 5 min, 400 ×g at room temperature. After two washes with DMEM and centrifugation for 5 min, 400 ×g at room temperature, a single-cell suspension in DMEM containing 10% (vol/vol) fetal bovine serum (ATCC) and 1% Penicillin Streptomycin (Thermo Fisher Scientific, Waltham, MA) was seeded in a 35-mm culture dish. After culturing in 5% CO₂ at 37°C for four days, most of the attached cells were RPE cells, which were cultured in complete DMEM for six more days. Cells that had reached confluence were subcultured at a 1:3 dilution in complete DMEM using trypsin-EDTA (0.25 trypsin, 2.21 mM EDTA). RPE cells were continued to be cultured in T75 flasks in complete DMEM and subcultured at a 1:3 dilution every three days until being used at passage 5 for the nuclear magnetic resonance (NMR) analysis. These cells were positive for RPE markers including pan-cytokeratin, tight junction protein, ZO-1, β-catenin, RPE65, and CRALBP (data not shown).

NMR sample preparation

RPE cells were cultured in triplicate to ~80% confluence. The medium was replaced with fresh medium 24 h before collection of cells. RPE cells in the T75 flask were washed twice with ice-cold PBS (pH 7.4), quenched using 3 ml methanol, and collected as described in Bhute *et al.*^{24–26} Intracellular metabolites were extracted using a dual phase extraction procedure adopted from Martineau *et al.*²⁷ Frozen brain and heart tissues were weighed and polar metabolites were extracted using a methanol-water-chloroform protocol described by Beckonert *et al.*²⁸ The samples were dried at 30°C using a vacuum concentrator and stored in –80°C.

For NMR analysis, samples were reconstituted in 0.6 ml of 0.1 M phosphate buffered D₂O (pH = 7.0) solution containing an internal standard (0.5 mM 3-trimethylsilyl-propionate-2, 2, 3, 3, -d₄ [TMSP, δ = 0.0 ppm]). Following centrifugation at 18,000 ×g for 10 min, the supernatant (550 μL) was transferred to NMR tubes (Norell Inc., Morgantown, NC).

NMR acquisition, data processing, and statistical analysis

¹H NMR spectra were recorded on a Bruker Avance III, exported to an ACD/1D NMR Processor (Advanced Chemistry Development), and processed as described in our previous study.²⁴ Peaks were annotated through the Human Metabolome Database (HMDB)²⁹ and Metabohunter.³⁰ Targeted profiling³¹ was performed using ChenomX NMR Suite Profiler (version 7.7, ChenomX Inc.). Metabolite concentrations were quantified as previously described²⁴ and exported as an Excel file (Microsoft). Metabolites with low confidence were excluded from the analysis. To evaluate the metabolite fractions and to account for the differences in efficiencies of

extraction, concentration data matrix for cultured RPE cells were further normalized by the total concentration of metabolites in each sample. In case of the tissues, the probabilistic quotient normalization (PQN) method³² was used for normalizing the metabolite concentrations. A list of metabolites identified in each tissue and cultured RPE cells is provided in Supplemental Table 1, and the complete data set including raw NMR files and processed data is available on MetaboLights server (ID: MTBLS1410).

The statistical analysis was performed using MetaboAnalyst 3.0.^{33,34} Unsupervised clustering was performed using principal component analysis (PCA) on the auto-scaled concentrations. Hierarchical clustering was performed on auto-scaled concentrations using Pearson's distance measure with ward clustering. Significantly altered metabolites ($P < 0.05$) between different genotypes were identified using one-way analysis of variance (ANOVA) with Tukey's HSD (honestly significant difference). Pathway topology analysis was performed for each genotype in the pathway analysis module of MetaboAnalyst using global test algorithm. Both relative betweenness centrality and outdegree centrality metrics were used to calculate the impact score of a pathway. Metabolic pathways with an impact score (either relative betweenness or outdegree) greater than 0 and false discovery rate (FDR) less than 0.05 were considered as significantly enriched. NMR spectral files as well as processed JCAMP files have been uploaded to MetaboLights database (ID: MTBLS1410), <http://www.ebi.ac.uk/metabolights/>.

Results

We used an ¹H NMR-based quantitative and targeted metabolic profiling³¹ to detect significant changes in metabolites in tissues and cultured RPE cells isolated from *Tmem135*^{FUN025/FUN025}, *Tmem135* TG, and WT (C57BL/6J) mice. The metabolites identified in these tissues and primary RPE cultures by NMR-based metabolomics are shown in Supplemental Table 1. The metabolites are classified into different groups based on either their functions or chemical structures.

Tmem135 mutation and overexpression significantly change metabolite concentrations in the heart

We first investigated the metabolic changes in the heart from the two models with modulation of *Tmem135*. Heart muscle cells derive the energy by fatty acid oxidation and therefore rely heavily on mitochondria for their function. Figure 1(a) shows the three-dimensional plot of PCA showing the first three principal components (PCs) of the NMR metabolomics assays. The metabolic profiles of the heart tissue from the three groups: WT, *Tmem135* TG, and *Tmem135*^{FUN025/FUN025} separated along the first PC (Figure 1(a)). Hierarchical clustering and PCA highlighted that the heart tissue from *Tmem135*^{FUN025/FUN025} mice showed greater variance when compared with heart tissues from WT and *Tmem135* TG. Importantly, samples from within the group clustered together, highlighting that the between-group differences are greater than within-group variations (Figure 1(b)). Sixteen metabolites were

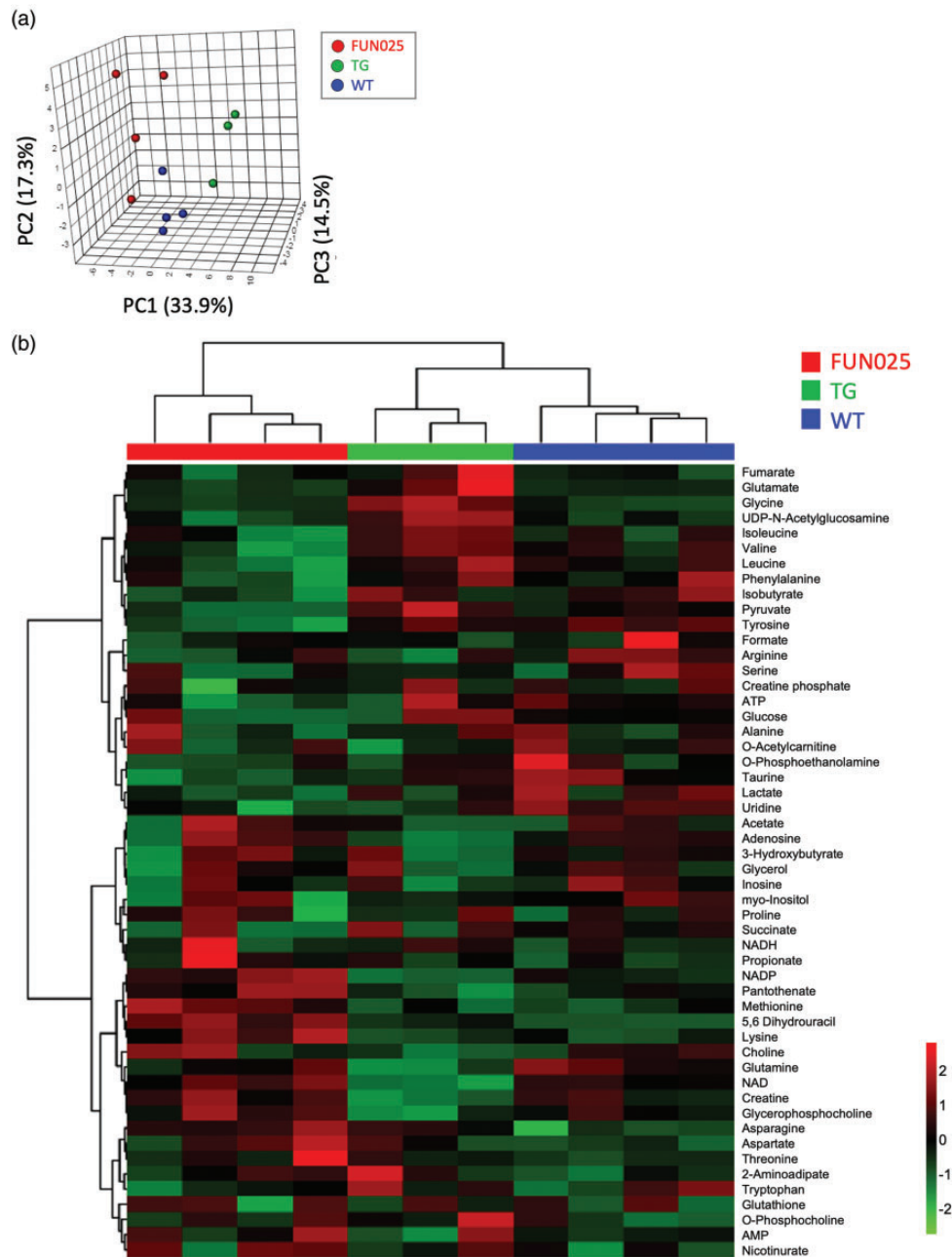


Figure 1. Heart metabolomics indicate significant metabolic changes due to modulation of *Tmem135*. (a) A three-dimensional PCA plot representing metabolite concentrations in heart tissues from *Tmem135*^{FUN025/FUN025} mice (red, $n = 4$), *Tmem135* TG mice (green, $n = 3$), and WT mice (blue, $n = 4$). Each data point represents data from individual animals. (b) Heat map showing hierarchical clustering using Pearson distance measure and ward linkage. The color in the heat map shows auto-scaled concentration (red-high, green-low). WT: wild type; FUN025: *Tmem135*^{FUN025/FUN025}; TG: *Tmem135* TG; PC: principal component; ATP: adenosine triphosphate.

significantly altered in different groups ($P < 0.05$, ANOVA followed by Tukey's *post hoc* method) (Figure 2(a) to (c)).

The heart tissue from *Tmem135*^{FUN025/FUN025} mice showed significant alterations in several essential amino acids, including lysine and methionine which were significantly increased, while valine and tyrosine were significantly reduced, as compared to the heart tissue from WT mice (Figure 2(b)). Asparagine was the non-essential amino acids which was also significantly increased in *Tmem135*^{FUN025/FUN025} versus WT mice (Figure 2(b)). More than two-fold increase was observed in 5,6-dihydrouracil

(Figure 2(c)), one of the metabolites involved in pyrimidine metabolism, and NADP^+ was also significantly increased in the heart tissue from *Tmem135*^{FUN025/FUN025} mice as compared to WT mice (Figure 2(c)).

Several metabolites associated with energy pathways were significantly altered in the hearts of *Tmem135* TG mice as compared to the hearts from WT mice. Specifically, creatine, the most abundant metabolite in the heart tissue, was significantly reduced in the hearts of *Tmem135* TG mice as compared to the hearts from WT mice (Figure 2(a)). Creatine is a key metabolite involved

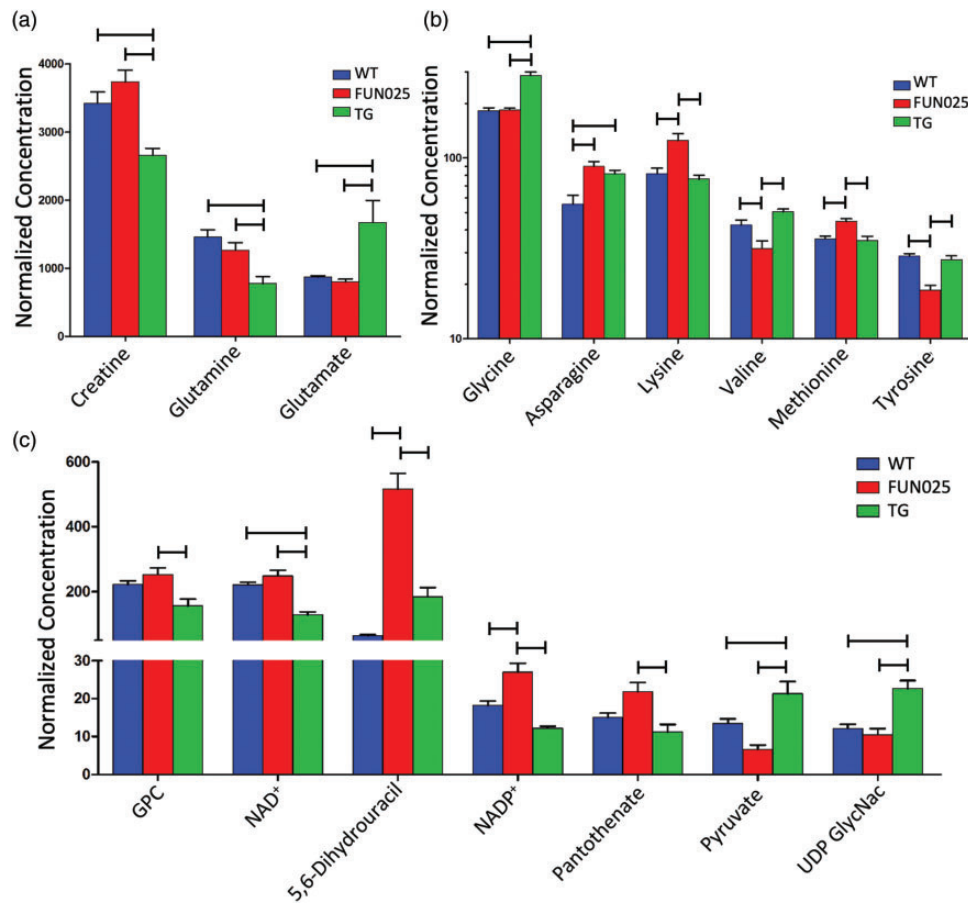


Figure 2. Normalized concentrations of significantly altered metabolites in the heart due to modulation of *Tmem135*. (a–c) Normalized concentrations of metabolites that are significantly altered in the heart due to *Tmem135* mutation or overexpression as tested by ANOVA followed by Tukey's HSD *post hoc* test ($P < 0.05$). Error bars represent SEM. PC: principal component; WT: wild type; FUN025: *Tmem135*^{FUN025/FUN025}; TG: *Tmem135* TG; GPC: glycerophosphocholine; UDP-GlycNac: UDP-N-Acetylglucosamine.

in the dynamic regulation of availability of adenosine triphosphate (ATP) by participating in the reaction catalyzed by creatine kinase that converts creatine and ATP to creatine phosphate and ADP. Since creatine is not synthesized in the heart, the reduced amount of creatine could be due to decreased creatine transport by the creatine transporter or increased use of creatine in the heart. A significant decrease in glutamine and a significant increase in glutamate were observed in the hearts of *Tmem135* TG mice (Figure 2(a)) indicating increased glutaminolysis, which is mostly a mitochondrial process,³⁵ relative to WT hearts. Among the amino acids, glycine and asparagine were also increased significantly in the hearts of *Tmem135* TG mice as compared to WT mice (Figure 2(b)). Asparagine is produced from aspartic acid catalyzed by asparagine synthetase, which also generates glutamate. It is possible that the observed increase in both asparagine and glutamate in *Tmem135* TG mice was due to this activity. NAD⁺, an important energy metabolite, was significantly reduced, while pyruvate and UDP-N-acetylglucosamine, products of glucose metabolism, accumulated in the hearts of *Tmem135* TG mice compared to WT mice (Figure 2(c)). These metabolomic data from the heart suggest that modulation of *Tmem135* significantly affects the metabolism in this tissue, which may lead to functional changes.

Brain tissues including hippocampus and cerebellum are not significantly affected by modulation of *Tmem135*

We next investigated the metabolic changes in tissues in the brain including hippocampus and cerebellum which were not found to show any robust phenotypes in *Tmem135* TG and *Tmem135*^{FUN025/FUN025} mice.^{19,20} We performed PCA on the metabolic profiles of the tissues from both *Tmem135* TG and *Tmem135*^{FUN025/FUN025} mice and observed that the metabolic profiles of hippocampus (Figure 3(a)) and cerebellum (Figure 3(b)) clustered together with the metabolic profiles of tissues from WT mice. This suggests that the within group variability was dominant and that modulation of *Tmem135* did not affect the global metabolic profiles in a significant manner in these tissues. This was also supported by hierarchical clustering (Supplemental Figure 1). ANOVA showed that glutamine and glycine were significantly decreased in the hippocampus of *Tmem135* TG mice (Figure 3(c)), while none of the metabolites were significantly affected (ANOVA, $P < 0.05$) in the cerebellum when compared to WT mice. Since, glutamine was significantly reduced in heart tissue and hippocampus of *Tmem135* TG mice, we examined the glutamine concentration in the cerebellum of these mice and observed a trend with reduced glutamine concentration ($P = 0.07$) (Figure 3(d)).

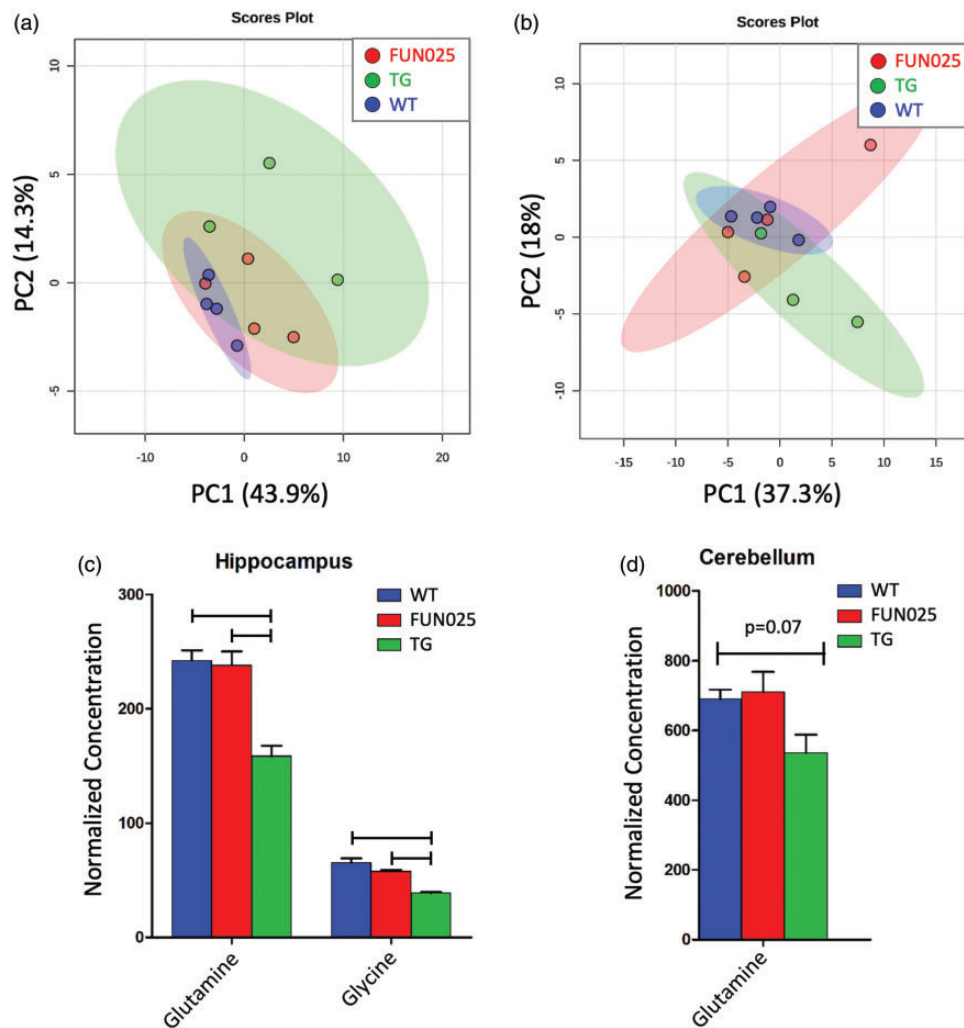


Figure 3. Brain metabolomics indicate negligible metabolic changes in hippocampus and cerebellum tissues due to modulation of *Tmem135*. Two-dimensional PCA plots representing metabolite concentrations in (a) hippocampus and (b) cerebellum of mice with different genotypes: *Tmem135*^{FUN025/FUN025} mice (red, $n = 4$), *Tmem135* TG mice (green, $n = 3$), and WT mice (blue, $n = 4$). Each data point represents data from individual animals and shaded region represents 95% confidence interval region. (c) Normalized concentrations of significantly altered metabolites in hippocampus, as tested by ANOVA followed by Tukey's HSD *post hoc* test ($P < 0.05$). Error bars represent SEM. (d) Normalized concentration of glutamine in cerebellum as a result of modulation of *Tmem135*. PC: principal component; WT: wild type; FUN025: *Tmem135*^{FUN025/FUN025}; TG: *Tmem135* TG.

***Tmem135* mutation and overexpression significantly change metabolite concentrations in cultured RPE cells**

Temporal characterization of phenotypes in the *Tmem135*^{FUN025/FUN025} retina indicated that the RPE, which is an active barrier that supports the neural retina in many ways,³⁶ appeared to be the initial cell layer affected.¹⁹ Increasing evidence also suggests that the RPE is the primary site of age-related macular degeneration (AMD) pathologies,^{37–39} presumably followed by secondary loss of photoreceptor cells.^{40,41} Considering mitochondria's essential roles in cellular metabolism, abnormal mitochondrial dynamics in *Tmem135* mouse models could very well affect the metabolism of RPE cells leading to functional abnormalities, which may in turn affect the health of photoreceptor cells. To investigate the influence of abnormal mitochondrial dynamics due to *Tmem135* mutation and overexpression on the metabolism of RPE cells, we isolated RPE cells from two-month-old *Tmem135*^{FUN025/FUN025},

Tmem135 TG, and WT mice and cultured them as previously described.^{19,23}

We performed PCA on the complete culture RPE cell metabolomics data set (Figure 4(a)) to cluster different samples based on their variance in the global metabolic profiles. Unsupervised PCA of the metabolomics data demonstrated a clear separation of three groups. Percent variance captured by PCA model for PC1 was 44.6%, and for PC2 was 26.2%. *Tmem135* TG clustered separately from WT along PC1 and PC2, while *Tmem135*^{FUN025/FUN025} was separated from WT along PC2. This suggests that significant metabolic changes are associated with the increased mitochondrial fission observed in *Tmem135* TG samples. Hierarchical clustering using Pearson correlation for distance metric and ward linkage method also supported the PCA data with cultured RPE cells isolated from *Tmem135* TG mice clustering separately from the other two groups (Figure 4(b)). Twenty-four metabolites were significantly altered in

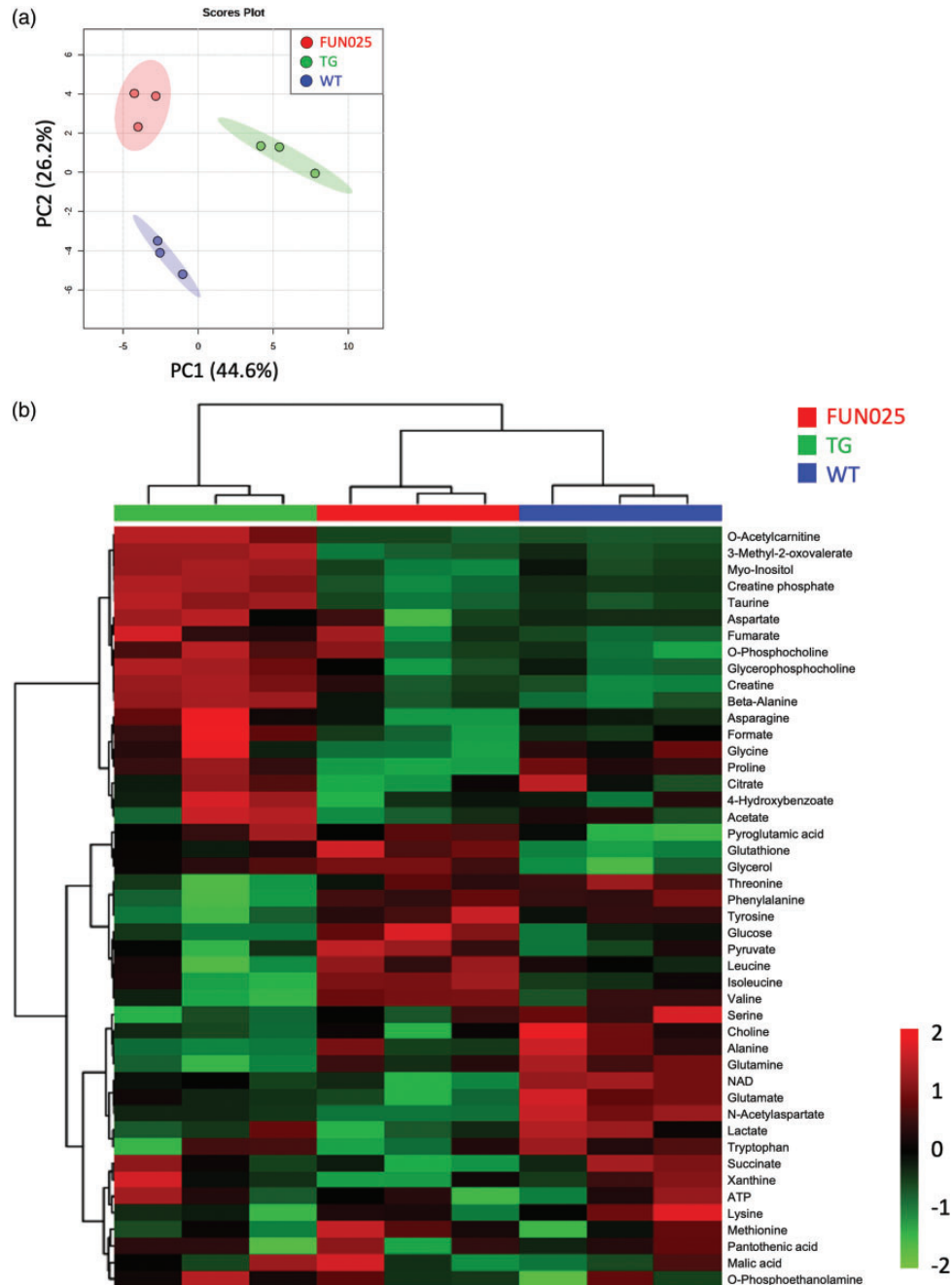


Figure 4. Cell culture metabolomics indicate significant metabolic changes due to modulation of *Tmem135* in RPE cells. (a) Two-dimensional PCA plots representing metabolite concentrations in cultured RPE cells isolated from mice with different genotypes: *Tmem135*^{FUN025/FUN025} (red), *Tmem135* TG mice (green), and WT mice (blue). Each data point represents biological replicates and shaded region represents 95% confidence interval region. (b) Heat map showing hierarchical clustering using Pearson distance measure and ward linkage. The color in the heat map shows auto-scaled concentration (red-high, green-low). PC: principal component; WT: wild type; FUN025: *Tmem135*^{FUN025/FUN025}; TG: *Tmem135* TG; ATP: adenosine triphosphate.

different groups ($P < 0.05$, ANOVA followed by Tukey's *post hoc* method) (Figure 5(a) to (d)).

In cultured RPE cells isolated from *Tmem135*^{FUN025/FUN025} mice, negligible changes were observed in essential amino acids as compared to WT cells (Figure 5(b)). Among the non-essential amino acids, glutamate and proline showed a significant decrease in abundance as compared to WT (Figure 5(a)). It has been shown that the most preferred nutrient consumed by RPE cells as an energy substrate is proline, which is exported to the apical side and

taken up by the neural retina (photoreceptor cells).⁴² A decrease of proline abundance suggests that *Tmem135*^{FUN025/FUN025} RPE may use more proline as the energy source or may alternatively uptake less proline from the environment. Creatine phosphate and N-acetylaspartate were significantly reduced, while glutathione was significantly increased in cultured RPE cells isolated from *Tmem135*^{FUN025/FUN025} mice as compared to WT cells among the amino acid derivatives (Figure 5(c)). Glucose and glycerol both were significantly increased while NAD⁺ was

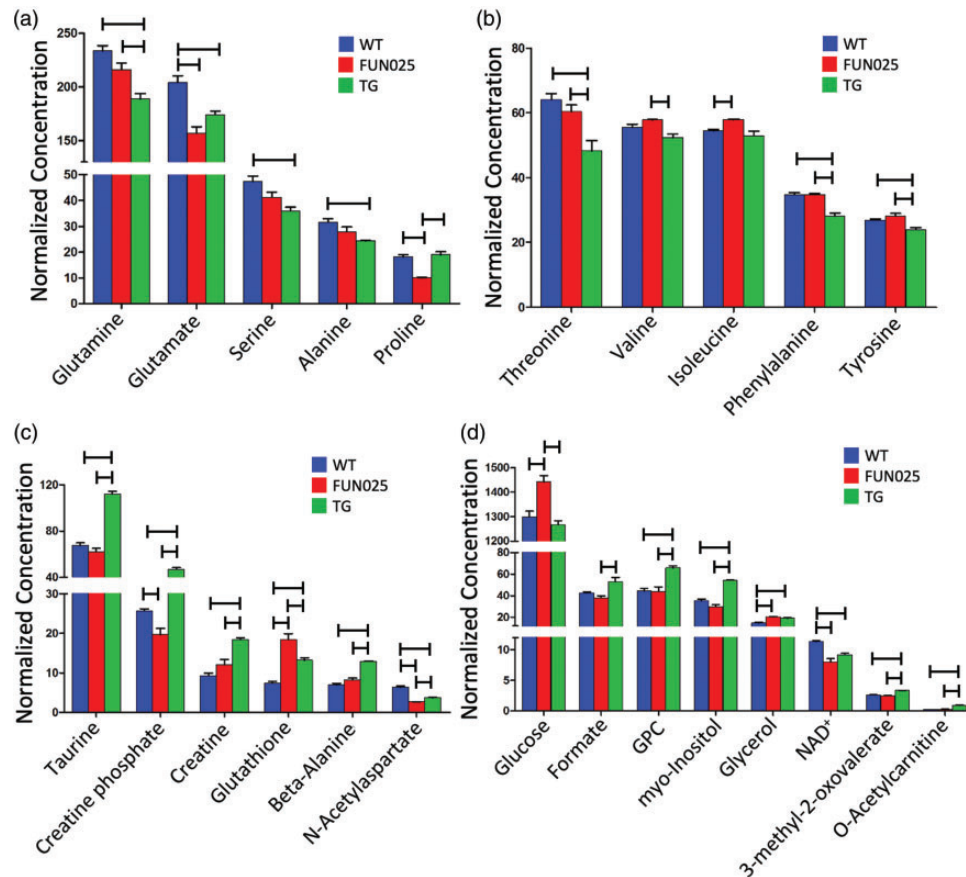


Figure 5. Normalized concentrations of significantly altered metabolites in RPE cells due to modulation of *Tmem135*. (a) Non-essential amino acids, (b) essential amino acids, (c) amino acid derivatives, and (d) other metabolites which are significantly altered, as tested by ANOVA followed by Tukey's HSD *post hoc* test ($P < 0.05$). Error bars represent SEM. WT: wild type; FUN025: *Tmem135*^{FUN025/FUN025}; TG: *Tmem135* TG; GPC: glycerophosphocholine.

significantly decreased in cultured RPE cells isolated from *Tmem135*^{FUN025/FUN025} mice as compared to WT cells (Figure 5(d)). These metabolic changes suggest that glucose and lipid metabolism may be affected in *Tmem135*^{FUN025/FUN025} RPE cells compared with WT RPE cells. Branched chain amino acids (BCAAs; valine, leucine, and isoleucine), which can also be used as energy sources in extra-hepatic tissues,⁴³ showed a trend towards accumulation in *Tmem135*^{FUN025/FUN025} RPE (Figure 5(b)). The levels of the BCAAs are upregulated in aged mouse blood,⁴⁴ suggesting that usage of BCAAs may change with aging. Recent study also found an increased accumulation of BCAAs in the brain of rats after ischemia-reperfusion (I/R) injury⁴⁵ suggesting a role of these amino acids in stressed tissues. The overall changes in these energy sources suggest alterations in energy production/utilization by *Tmem135*^{FUN025/FUN025} RPE cells relative to WT RPE cells. This may have impact on the normal function of RPE cells, which in turn could lead to age-related retinal phenotypes observed in *Tmem135*^{FUN025/FUN025} mice.¹⁹

In cultured RPE cells isolated from *Tmem135* TG mice, abundances of several non-essential amino acids (glutamine, glutamate, serine, and alanine, Figure 5(a)) and essential amino acids (threonine, phenylalanine, and tyrosine, Figure 5(b)) were significantly decreased as compared

to WT. Similar to the tissues we examined, glutamine concentration was decreased in cultured RPE cells isolated from *Tmem135* TG mice highlighting a tissue-independent effect of *Tmem135* overexpression. Several amino acid derivatives including taurine, creatine, creatine phosphate, glutathione, and beta-alanine were significantly increased in RPE cells derived from *Tmem135* TG mice as compared to WT (Figure 5(c)). A decrease in essential and non-essential amino acids together with an increase in their metabolites indicate increased amino acid metabolism in *Tmem135* TG RPE cells relative to WT RPE cells. An amino acid derivative, N-acetylaspartate, was decreased in *Tmem135* TG RPE cells (Figure 5(c)). Taurine, beta-alanine, myo-inositol, and glycerophosphocholine, which also serve osmoregulatory functions are increased in *Tmem135* TG RPE cells (Figure 5(c) and (d)) suggesting that RPE cells are experiencing osmotic stress. Hyperosmotic stress may trigger cell shrinkage, oxidative stress, protein carbonylation, mitochondrial depolarization, DNA damage, and cell cycle arrest, thus rendering cells susceptible to apoptosis.⁴⁶ Beta alanine is also a precursor of several amino acid derivatives including pantothenic acid (precursor of acetyl coenzyme A synthesis), uracil (pyrimidine metabolism), spermine (polyamine metabolism and arginine metabolism), malonate (fatty acid metabolism), and carnosine (a reactive

oxygen species scavenging molecule and suppressor of production of advanced glycation end products).⁴⁷⁻⁴⁹ Increase in total beta-alanine concentration indicates impaired conversion of beta-alanine into these derivatives in *Tmem135* TG RPE cells, which can have significant impact on related metabolic pathways and affect the health of these cells. Among other metabolites, glycerol was increased while NAD⁺ was decreased in *Tmem135* TG RPE cells compared to WT RPE cells (Figure 5(d)).

Pathway analysis for predicting metabolic pathways affected in RPE cells and the heart

Changes in the steady-state metabolite concentrations can be useful for identifying potential metabolic pathways that are altered or enriched in the two models affecting the activity of *Tmem135*. We used the pathway topology analysis to identify metabolic pathways that are likely affected (FDR < 0.05) in cultured RPE cells (Figure 6(a)) as well as heart tissues (Figure 6(b)) from *Tmem135* TG and *Tmem135*^{FUN025/FUN025} mice relative to WT mice. We observed a greater number of metabolic pathways which were enriched in *Tmem135* TG (23 relative to WT) RPE cells as compared to *Tmem135*^{FUN025/FUN025} (14 relative to WT) RPE cells (Figure 6(a)). Similarly, a greater number of

metabolic pathways were found to be significantly enriched in *Tmem135* TG heart (15 relative to WT) as compared to *Tmem135*^{FUN025/FUN025} heart (10 relative to WT) (Figure 6(b)).

Metabolic pathways significantly enriched in RPE cells as well as the heart tissue of both *Tmem135*^{FUN025/FUN025} and *Tmem135* TG genotypes (Figure 6) include pyrimidine metabolism, arginine and proline metabolism, alanine, aspartate and glutamate metabolism, and protein synthesis (aminoacyl-tRNA biosynthesis). These metabolic pathways may be generally closely associated with and sensitive to changes in *Tmem135* and/or mitochondrial dynamics across different tissues and cell types. Both *Tmem135* TG and *Tmem135*^{FUN025/FUN025} RPE cells showed significant enrichment in glycine, serine and threonine metabolism, glutathione metabolism, nicotinate and nicotinamide metabolism, galactose metabolism, glycerolipid metabolism, and nitrogen metabolism. These pathways may represent ones that are sensitive to *Tmem135* gene modulation and/or mitochondrial dynamics changes in RPE cells. Beta-alanine metabolism was enriched in both *Tmem135* TG and *Tmem135*^{FUN025/FUN025} heart relative to WT heart in addition to aforementioned pathways, indicating that this pathway is sensitive to *Tmem135* modulation and/or mitochondrial dynamics alterations in the heart.

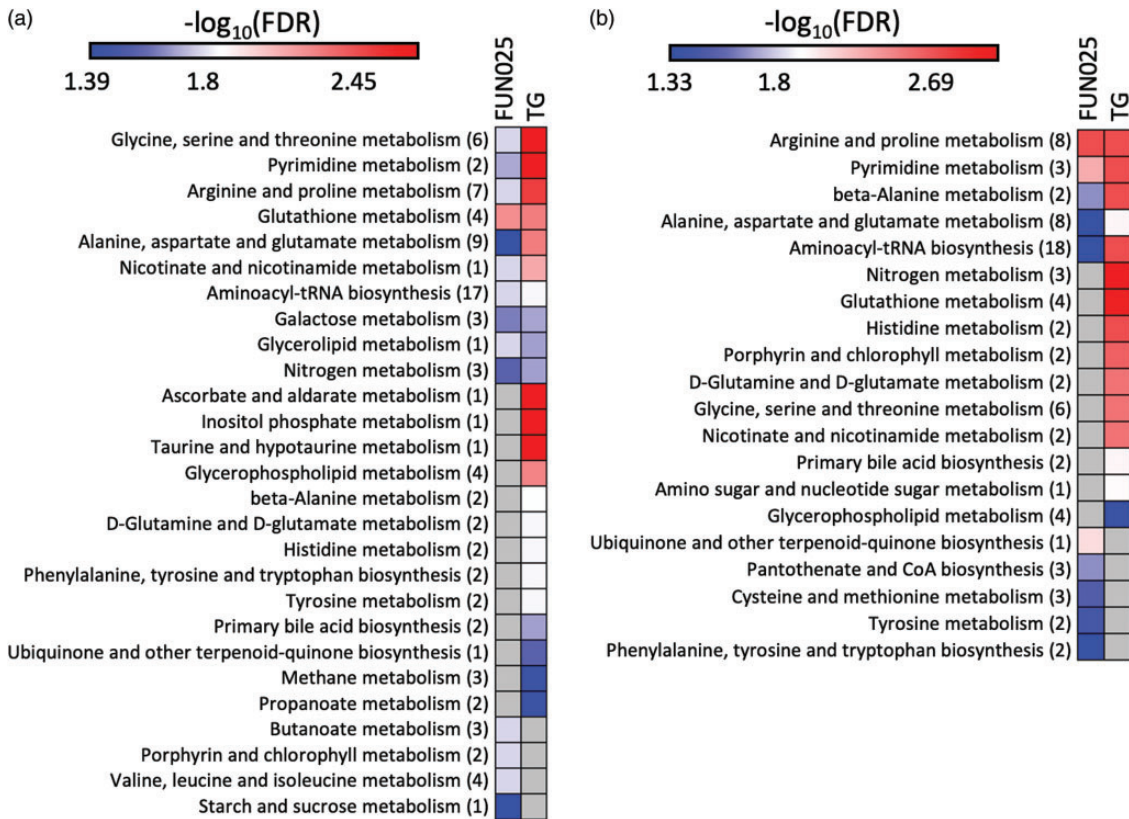


Figure 6. Pathway analysis identifies significantly enriched pathways due to modulation of *Tmem135* in cultured RPE cells and heart tissue. Heat map showing metabolic pathways which are significantly enriched in the (a) cultured RPE cells and (b) heart tissues of mice with different genotypes: *Tmem135*^{FUN025/FUN025} relative to WT mice (FUN025) and *Tmem135* TG relative to WT mice (TG). The color in the heat map represents $-\log_{10}(\text{FDR})$ (red: highly significant) and brackets next to pathways indicate the number of metabolites which are matched in the pathway and metabolic analysis. Pathways are considered significantly enriched if FDR < 0.05 and impact > 0. Impact score indicates the impact of significantly affected metabolites in the pathway based on network topology measure defined as a sum of relative betweenness centrality and outdegree centrality. WT: wild type; FUN025: *Tmem135*^{FUN025/FUN025}; TG: *Tmem135* TG; FDR: false discovery rate; tRNA: transfer ribonucleic acid.

Discussion

Mitochondrial integrity is critical for healthy aging process. Several age-related diseases/pathologies have been associated with aberrant mitochondrial dynamics including neurodegeneration, metabolic syndromes, and cardiovascular disease.⁵⁰ Our previous studies had identified TMEM135, a protein important for regulating mitochondrial dynamics, to be associated with age-related diseases/pathologies. AMD-like phenotypes were observed in *Tmem135*^{FUN025} mutant mice,¹⁹ while cardiomyopathy was observed in mice with *Tmem135* overexpression.²⁰ Our *Tmem135* mouse models (with a mutation and overexpression of *Tmem135*) can be useful tools to understand the underlying causes as well as to develop potential treatment strategies for these pathologies. To further characterize these models, the metabolic profiles of tissues and RPE cells of *Tmem135*^{FUN025/FUN025} (fusion>fission) and *Tmem135* TG (fusion<fission) mice were investigated in this study.

Metabolomic analysis of different tissues and cells from *Tmem135*^{FUN025/FUN025} and *Tmem135* TG mice indicated that metabolic changes due to modulation of *Tmem135* occur in a tissue-specific manner. We observed that while heart and RPE cells showed high sensitivity to changes in *Tmem135* expression, brain tissues including hippocampus and cerebellum showed negligible metabolic changes. We identified several metabolic changes associated with different genotypes as well as potential metabolic pathways which are likely affected in the heart as well as RPE cells isolated from either *Tmem135*^{FUN025/FUN025} or *Tmem135* TG mice. These data provide evidence that metabolic profiling can be used to characterize the tissues which are sensitive to *Tmem135* modulation and also to identify potential metabolic pathways which may be associated with increased fission (overexpression of *Tmem135*) or increased fusion (mutant *Tmem135*) of mitochondria in those tissues showing affected phenotypes. We cannot exclude the possibility that tissue-specific metabolic changes may be partly due to differences in the expression level of the *Tmem135* transgene. It will be of great interest to investigate whether and how these metabolic changes lead to mitochondria and age-related pathologies of RPE cells as well as the heart abnormalities.

Some of the metabolic changes were commonly observed between multiple tissues and/or across different genotypes, which may have unique implications. For example, glutamine was reduced in both the heart and RPE cells as well as hippocampus from *Tmem135* TG mice. In the *Tmem135* TG heart, a significant increase in glutamate was also observed, indicating increased glutaminolysis. Glutaminolysis is mostly a mitochondrial process that converts glutamine to glutamate.³⁵ Glutamate is a major excitatory neurotransmitter, and is used for the synthesis of the antioxidant glutathione or further metabolized to α -keto-glutarate to generate ATP in the Krebs cycle. *Tmem135* TG heart tissue may utilize more glutamine for antioxidant reaction or as an extra energy source. It is interesting to note that glutamine-to-glutamate ratio in the plasma is inversely associated with metabolic disease parameters.^{51–54} Since glutamine concentration is affected

significantly in different tissues of *Tmem135* TG mice (which show increased mitochondrial fission as compared to fusion), it is likely that glutamine metabolism is sensitive to mitochondrial fission. Our pathway analysis indicated that there are more metabolic changes that are common between the *Tmem135* TG heart and RPE cells. Thirteen out of the 15 metabolic pathways which were significantly enriched in the heart tissue of *Tmem135* TG mice (relative to WT mice) were also significantly enriched in the cultured RPE cells isolated from *Tmem135* TG mice (relative to WT mice). Those metabolic pathways commonly enriched in both RPE cells and the heart of *Tmem135* TG mice may be associated with fragmented mitochondria and/or phenotypic abnormalities observed in *Tmem135* TG mice.²⁰

Cultured RPE cells isolated from both *Tmem135* TG and *Tmem135*^{FUN025/FUN025} mice showed significant decreases in NAD⁺, N-acetylaspartate, and glutamate and significant increases in glutathione and glycerol, suggesting that these metabolic changes are likely associated with disruption of homeostasis of mitochondrial dynamics in RPE cells. Increases in glycerol abundances in both *Tmem135*^{FUN025/FUN025} and *Tmem135* TG RPE cells suggest that the lipid metabolism may be disrupted in these cells. While metabolisms of lipid, glucose and BCAA are all affected in *Tmem135*^{FUN025/FUN025} RPE, only lipid metabolism seems to be mainly affected in *Tmem135* TG RPE cells. Association between the fat storage organelles, lipid droplets, and mitochondria has been observed with fused/elongated mitochondria,^{55,56} suggesting the connection between the lipid metabolism and mitochondrial dynamics. A reduction in N-acetylaspartate (Figure 5(c)), a metabolite which is synthesized from aspartate and acetyl-coenzyme A in the mitochondria, is also observed in both *Tmem135*^{FUN025/FUN025} and *Tmem135* TG RPE cells, which may be attributed to a reduction in its synthesis rate owing to changes in mitochondrial function. An increase in glutathione (Figure 5(c)) and a decrease in glutamate (Figure 5(a)) could be attributed to increased synthesis of glutathione owing to increased oxidative stress.⁵⁷ Indeed, our previous study indicated that the level of oxidative stress was increased in both *Tmem135*^{FUN025/FUN025} and *Tmem135* TG fibroblast cells.¹⁹ Increase in glutathione suggests that oxidative stress is similarly increased in *Tmem135*^{FUN025/FUN025} and *Tmem135* TG RPE cells due to abnormal mitochondrial dynamics. Increased oxidative stress can also lead to an increased DNA damage and over-activation of poly (ADP-ribose) polymerase (PARP) activity. PARP1 is known to be a major consumer of NAD⁺, which may result in a decrease in total NAD⁺ concentrations in the cells. Indeed, *Tmem135*^{FUN025/FUN025} RPE cells show significantly higher PARP1 activity compared to WT RPE cells, while *Tmem135* TG RPE cells also show a higher trend (Supplemental Figure 2). Increased PARP1 activity may be at least in part responsible for the decrease in NAD⁺ concentration in *Tmem135*^{FUN025/FUN025} and *Tmem135* TG RPE cells. NAD⁺ is a critical metabolic cofactor that regulates cellular metabolic homeostasis. NAD⁺ is involved in cellular ATP production through oxidative phosphorylation, and regulates various enzymes involved in metabolic pathways.⁴⁵ It has been shown that the level of

NAD⁺ decreases during aging in worms, rodents, and humans.^{58–61} In addition, reduction of NAD⁺ or NAD⁺/NADH ratio is associated with mitochondrial diseases and age-related disorders including neurodegeneration, obesity and diabetes, and cancer.^{62–65} Therefore, it will be of interest to test if depletion of NAD⁺ is responsible for some of the RPE abnormalities in *Tmem135*^{FLN025/FLN025} and *Tmem135* TG mice, and underlies age-related retinal disease phenotypes including inflammation and neurodegeneration as future studies.

Authors' contributions: All authors participated in the design, interpretation of the studies, and analysis of the data and review of the manuscript. WHL, VJB, and HH conducted the experiments, WHL, VJB, SI, SPP, and AI wrote the manuscript. WHL and VJB contributed equally to this paper.

ACKNOWLEDGEMENT

The authors thank Michael Landowski for critical review of the manuscript.



DECLARATION OF CONFLICTING INTERESTS

The author(s) declared no potential conflicts of interest with respect to the research, authorship, and/or publication of this article.

FUNDING

The author(s) disclosed receipt of the following financial support for the research, authorship, and/or publication of this article: This work was supported by funding from the National Institutes of Health (NIH) (R01 EY022086) and Timothy William Trout Professorship to AI. Support by NIH (R01 HL148059) and the National Science Foundation Center for Cell Manufacturing Technologies (EEC-1648035) to SPP is also acknowledged.

ORCID iDs

Hitoshi Higuchi  <https://orcid.org/0000-0002-8600-7793>
Akihiro Ikeda  <https://orcid.org/0000-0001-8440-3891>

SUPPLEMENTAL MATERIAL

Supplemental material for this article is available online.

REFERENCES

- Chen H, Detmer SA, Ewald AJ, Griffin EE, Fraser SE, Chan DC. Mitofusins Mfn1 and Mfn2 coordinately regulate mitochondrial fusion and are essential for embryonic development. *J Cell Biol* 2003;**160**:189–200
- Olichon A, Guillou E, Delettre C, Landes T, Arnaune-Pelloquin L, Emorine LJ, Mills V, Daloyau M, Hamel C, Amati-Bonneau P, Bonneau D, Reynier P, Lenaers G, Belenguer P. Mitochondrial dynamics and disease, OPA1. *Biochim Biophys Acta* 2006;**1763**:500–9
- Mears JA, Lackner LL, Fang S, Ingerman E, Nunnari J, Hinshaw JE. Conformational changes in Dnm1 support a contractile mechanism for mitochondrial fission. *Nat Struct Mol Biol* 2011;**18**:20–6
- Bernhardt D, Muller M, Reichert AS, Osiewacz HD. Simultaneous impairment of mitochondrial fission and fusion reduces mitophagy and shortens replicative lifespan. *Sci Rep* 2015;**5**:7885
- Yang CC, Chen D, Lee SS, Walter L. The dynamin-related protein DRP-1 and the insulin signaling pathway cooperate to modulate *Caenorhabditis elegans* longevity. *Aging Cell* 2011;**10**:724–8
- McQuibban GA, Lee JR, Zheng L, Juusola M, Freeman M. Normal mitochondrial dynamics requires rhomboid-7 and affects drosophila lifespan and neuronal function. *Curr Biol* 2006;**16**:982–9
- Wangler MF, Assia Batzir N, Robak LA, Koenig MK, Bacino CA, Scaglia F, Bellen HJ. The expanding neurological phenotype of DNM1L-related disorders. *Brain* 2018;**141**:e28
- El-Hattab AW, Suleiman J, Almannai M, Scaglia F. Mitochondrial dynamics: biological roles, molecular machinery, and related diseases. *Mol Genet Metab* 2018;**125**:315–21
- Zuchner S, Mersyanova IV, Muglia M, Bissar-Tadmouri N, Rochelle J, Dadali EL, Zappia M, Nelis E, Patitucci A, Senderek J, Parman Y, Evgrafov O, Jonghe PD, Takahashi Y, Tsuji S, Pericak-Vance MA, Quattrone A, Battaloglu E, Polyakov AV, Timmerman V, Schroder JM, Vance JM. Mutations in the mitochondrial GTPase mitofusin 2 cause Charcot-Marie-Tooth neuropathy type 2A. *Nat Genet* 2004;**36**:449–51
- Rouzier C, Bannwarth S, Chaussonot A, Chevrollier A, Verschueren A, Bonello-Palot N, Fragaki K, Cano A, Pouget J, Pellissier JF, Procaccio V, Chabrol B, Paquis-Flucklinger V. The MFN2 gene is responsible for mitochondrial DNA instability and optic atrophy 'plus' phenotype. *Brain* 2012;**135**:23–34
- Amati-Bonneau P, Valentino ML, Reynier P, Gallardo ME, Bornstein B, Boissiere A, Campos Y, Rivera H, de la Aleja JG, Carroccia R, Iommarini L, Labauge P, Figarella-Branger D, Marcocelles P, Furby A, Beauvais K, Letournel F, Liguori R, La Morgia C, Montagna P, Liguori M, Zanna C, Rugolo M, Cossarizza A, Wissinger B, Verny C, Schwarzenbacher R, Martin MA, Arenas J, Ayuso C, Garesse R, Lenaers G, Bonneau D, Carelli V. OPA1 mutations induce mitochondrial DNA instability and optic atrophy 'plus' phenotypes. *Brain* 2008;**131**:338–51
- Gerber S, Charif M, Chevrollier A, Chaumette T, Angebault C, Kane MS, Paris A, Alban J, Quiles M, Delettre C, Bonneau D, Procaccio V, Amati-Bonneau P, Reynier P, Lerulez S, Calmon R, Boddaert N, Funalot B, Rio M, Bouccara D, Meunier I, Sesaki H, Kaplan J, Hamel CP, Rozet JM, Lenaers G. Mutations in DNM1L, as in OPA1, result in dominant optic atrophy despite opposite effects on mitochondrial fusion and fission. *Brain* 2017;**140**:2586–96
- Song M, Mihara K, Chen Y, Scorrano L, Dorn GW 2nd. Mitochondrial fission and fusion factors reciprocally orchestrate mitophagic culling in mouse hearts and cultured fibroblasts. *Cell Metab* 2015;**21**:273–86
- Wai T, Garcia-Prieto J, Baker MJ, Merkwirth C, Benit P, Rustin P, Ruperez FJ, Barbas C, Ibanez B, Langer T. Imbalanced OPA1 processing and mitochondrial fragmentation cause heart failure in mice. *Science* 2015;**350**:aad0116
- Spinelli JB, Haigis MC. The multifaceted contributions of mitochondria to cellular metabolism. *Nat Cell Biol* 2018;**20**:745–54
- Morava E, van den Heuvel L, Hol F, de Vries MC, Hogeveen M, Rodenburg RJ, Smeitink JA. Mitochondrial disease criteria: diagnostic applications in children. *Neurology* 2006;**67**:1823–6
- Schaefer AM, Taylor RW, Turnbull DM, Chinnery PF. The epidemiology of mitochondrial disorders—past, present and future. *Biochim Biophys Acta* 2004;**1659**:115–20
- Exil VJ, Silva Avila D, Benedetto A, Exil EA, Adams MR, Au C, Aschner M. Stressed-induced TMEM135 protein is part of a conserved genetic network involved in fat storage and longevity regulation in *Caenorhabditis elegans*. *PLoS One* 2010;**5**:e14228
- Lee WH, Higuchi H, Ikeda S, Macke EL, Takimoto T, Pattnaik BR, Liu C, Chu LF, Siepka SM, Krentz KJ, Rubinstein CD, Kalejta RF, Thomson JA, Mullins RF, Takahashi JS, Pinto LH, Ikeda A. Mouse *Tmem135* mutation reveals a mechanism involving mitochondrial dynamics that leads to age-dependent retinal pathologies. *Elife* 2016;**5**:e19264
- Lewis SA, Takimoto T, Mehrvar S, Higuchi H, Doebley AL, Stokes G, Sheibani N, Ikeda S, Ranji M, Ikeda A. The effect of *Tmem135* over-expression on the mouse heart. *PLoS One* 2018;**13**:e0201986
- Pinto LH, Vitaterna MH, Siepka SM, Shimomura K, Lumayag S, Baker M, Fenner D, Mullins RF, Sheffield VC, Stone EM, Heffron E, Takahashi JS. Results from screening over 9000 mutation-bearing mice for defects

- in the electroretinogram and appearance of the fundus. *Vision Res* 2004;**44**:3335–45
22. Vitaterna MH, Pinto LH, Takahashi JS. Large-scale mutagenesis and phenotypic screens for the nervous system and behavior in mice. *Trends Neurosci* 2006;**29**:233–40
 23. Chen M, Muckersie E, Robertson M, Fraczek M, Forrester JV, Xu H. Characterization of a spontaneous mouse retinal pigment epithelial cell line B6-RPE07. *Invest Ophthalmol Vis Sci* 2008;**49**:3699–706
 24. Bhute VJ, Bao X, Dunn KK, Knutson KR, McCurry EC, Jin G, Lee WH, Lewis S, Ikeda A, Palecek SP. Metabolomics identifies metabolic markers of maturation in human pluripotent stem Cell-Derived cardiomyocytes. *Theranostics* 2017;**7**:2078–91
 25. Bhute VJ, Palecek SP. Metabolic responses induced by DNA damage and poly (ADP-ribose) polymerase (PARP) inhibition in MCF-7 cells. *Metabolomics* 2015;**11**:1779–91
 26. Bhute VJ, Ma Y, Bao X, Palecek SP. The poly (ADP-Ribose) polymerase inhibitor veliparib and radiation cause significant cell line dependent metabolic changes in breast cancer cells. *Sci Rep* 2016;**6**:36061
 27. Martineau E, Tea I, Loac G, Giraudeau P, Akoka S. Strategy for choosing extraction procedures for NMR-based metabolomic analysis of mammalian cells. *Anal Bioanal Chem* 2011;**401**:2133–42
 28. Beckonert O, Keun HC, Ebbels TM, Bundy J, Holmes E, Lindon JC, Nicholson JK. Metabolic profiling, metabolomic and metabonomic procedures for NMR spectroscopy of urine, plasma, serum and tissue extracts. *Nat Protoc* 2007;**2**:2692–703
 29. Wishart DS, Jewison T, Guo AC, Wilson M, Knox C, Liu Y, Djoumbou Y, Mandal R, Aziat F, Dong E, Bouatra S, Sinelnikov I, Arndt D, Xia J, Liu P, Yallou F, Bjorn Dahl T, Perez-Pineiro R, Eisner R, Allen F, Neveu V, Greiner R, Scalbert A. HMDB 3.0—the human metabolome database in 2013. *Nucleic Acids Res* 2013;**41**:D801–7
 30. Tulpan D, Leger S, Belliveau L, Culf A, Cuperlovic-Culf M. MetaboHunter: an automatic approach for identification of metabolites from 1H-NMR spectra of complex mixtures. *BMC Bioinformatics* 2011;**12**:400
 31. Weljie AM, Newton J, Mercier P, Carlson E, Slupsky CM. Targeted profiling: quantitative analysis of 1H NMR metabolomics data. *Anal Chem* 2006;**78**:4430–42
 32. Dieterle F, Ross A, Schlotterbeck G, Senn H. Probabilistic quotient normalization as robust method to account for dilution of complex biological mixtures. Application in 1H NMR metabolomics. *Anal Chem* 2006;**78**:4281–90
 33. Xia J, Mandal R, Sinelnikov IV, Broadhurst D, Wishart DS. MetaboAnalyst 2.0 – a comprehensive server for metabolomic data analysis. *Nucleic Acids Res* 2012;**40**:W127–33
 34. Xia J, Sinelnikov IV, Han B, Wishart DS. MetaboAnalyst 3.0 – making metabolomics more meaningful. *Nucleic Acids Res* 2015;**43**:W251–7
 35. Mates JM, Segura JA, Campos-Sandoval JA, Lobo C, Alonso L, Alonso FJ, Marquez J. Glutamine homeostasis and mitochondrial dynamics. *Int J Biochem Cell Biol* 2009;**41**:2051–61
 36. Rizzolo LJ, Peng S, Luo Y, Xiao W. Integration of tight junctions and claudins with the barrier functions of the retinal pigment epithelium. *Prog Retin Eye Res* 2011;**30**:296–323
 37. Ambati J, Atkinson JP, Gelfand BD. Immunology of age-related macular degeneration. *Nat Rev Immunol* 2013;**13**:438–51
 38. de Jong PT. Age-related macular degeneration. *N Engl J Med* 2006;**355**:1474–85
 39. Terluk MR, Kapphahn RJ, Soukup LM, Gong H, Gallardo C, Montezuma SR, Ferrington DA. Investigating mitochondria as a target for treating age-related macular degeneration. *J Neurosci* 2015;**35**:7304–11
 40. Roth F, Bindewald A, Holz FG. Keypathophysiologic pathways in age-related macular disease. *Graefes Arch Clin Exp Ophthalmol* 2004;**242**:710–6
 41. Bonilha VL. Age and disease-related structural changes in the retinal pigment epithelium. *Clin Ophthalmol* 2008;**2**:413–24
 42. Chao JR, Knight K, Engel AL, Jankowski C, Wang Y, Manson MA, Gu H, Djukovic D, Raftery D, Hurley JB, Du J. Human retinal pigment epithelial cells prefer proline as a nutrient and transport metabolic intermediates to the retinal side. *J Biol Chem* 2017;**292**:12895–905
 43. Harper AE, Miller RH, Block KP. Branched-chain amino acid metabolism. *Annu Rev Nutr* 1984;**4**:409–54
 44. Houtkooper RH, Argmann C, Houten SM, Canto C, Jenjina EH, Andreux PA, Thomas C, Doenlen R, Schoonjans K, Auwerx J. The metabolic footprint of aging in mice. *Sci Rep* 2011;**1**:134
 45. Wesley UV, Bhute VJ, Hatcher JF, Palecek SP, Dempsey RJ. Local and systemic metabolic alterations in brain, plasma, and liver of rats in response to aging and ischemic stroke, as detected by nuclear magnetic resonance (NMR) spectroscopy. *Neurochem Int* 2019;**127**:113–24
 46. Brocker C, Thompson DC, Vasilou V. The role of hyperosmotic stress in inflammation and disease. *Biomol Concepts* 2012;**3**:345–64
 47. Boldyrev A, Bulygina E, Leinsoo T, Petrushanko I, Tsubone S, Abe H. Protection of neuronal cells against reactive oxygen species by carnosine and related compounds. *Comp Biochem Physiol B, Biochem Mol Biol* 2004;**137**:81–8
 48. Hipkiss AR, Brownson C, Bertani MF, Ruiz E, Ferro A. Reaction Of carnosine with aged proteins: another protective process?. *Ann N Y Acad Sci* 2002;**959**:285–94
 49. Pfister F, Riedl E, Wang Q, Vom Hagen F, Deinzer M, Harmsen MC, Molema G, Yard B, Feng Y, Hammes HP. Oral carnosine supplementation prevents vascular damage in experimental diabetic retinopathy. *Cell Physiol Biochem* 2011;**28**:125–36
 50. Sebastian D, Palacin M, Zorzano A. Mitochondrial dynamics: coupling mitochondrial fitness with healthy aging. *Trends Mol Med* 2017;**23**:201–15
 51. Newgard CB, An J, Bain JR, Muehlbauer MJ, Stevens RD, Lien LF, Haqq AM, Shah SH, Arlotto M, Slentz CA, Rochon J, Gallup D, Ilkayeva O, Wenner BR, Yancy WS Jr, Eisenson H, Musante G, Surwit RS, Millington DS, Butler MD, Svetkey LP. A branched-chain amino acid-related metabolic signature that differentiates obese and lean humans and contributes to insulin resistance. *Cell Metab* 2009;**9**:311–26
 52. Tai ES, Tan ML, Stevens RD, Low YL, Muehlbauer MJ, Goh DL, Ilkayeva OR, Wenner BR, Bain JR, Lee JJ, Lim SC, Khoo CM, Shah SH, Newgard CB. Insulin resistance is associated with a metabolic profile of altered protein metabolism in chinese and Asian-Indian men. *Diabetologia* 2010;**53**:757–67
 53. Wurtz P, Mäkinen VP, Soininen P, Kangas AJ, Tukiainen T, Kettunen J, Savolainen MJ, Tammelin T, Viikari JS, Ronnema T, Kahonen M, Lehtimäki T, Ripatti S, Raitakari OT, Jarvelin MR, Ala-Korpela M. Metabolic signatures of insulin resistance in 7,098 young adults. *Diabetes* 2012;**61**:1372–80
 54. McCormack SE, Shaham O, McCarthy MA, Deik AA, Wang TJ, Gerszten RE, Clish CB, Mootha VK, Grinspoon SK, Fleischman A. Circulating branched-chain amino acid concentrations are associated with obesity and future insulin resistance in children and adolescents. *Pediatr Obes* 2013;**8**:52–61
 55. Rambold AS, Cohen S, Lippincott-Schwartz J. Fatty acid trafficking in starved cells: regulation by lipid droplet lipolysis, autophagy, and mitochondrial fusion dynamics. *Dev Cell* 2015;**32**:678–92
 56. Benador IY, Veliova M, Mahdaviyani K, Petcherski A, Wikstrom JD, Assali EA, Acin-Perez R, Shum M, Oliveira MF, Cintii S, Sztalryd C, Barshop WD, Wohlschlegel JA, Corkey BE, Liesa M, Shirihai OS. Mitochondria bound to lipid droplets have unique bioenergetics, composition, and dynamics that support lipid droplet expansion. *Cell Metab* 2018;**27**:869–85.e6
 57. Lu SC. Glutathione synthesis. *Biochim Biophys Acta* 2013;**1830**:3143–53
 58. Braidy N, Guillemin GJ, Mansour H, Chan-Ling T, Poljak A, Grant R. Age related changes in NAD+ metabolism oxidative stress and Sirt1 activity in wistar rats. *PLoS One* 2011;**6**:e19194
 59. Gomes AP, Price NL, Ling AJ, Moslehi JJ, Montgomery MK, Rajman L, White JP, Teodoro JS, Wrann CD, Hubbard BP, Mercken EM, Palmeira CM, de Cabo R, Rolo AP, Turner N, Bell EL, Sinclair DA. Declining NAD(+) induces a pseudohypoxic state disrupting nuclear-mitochondrial communication during aging. *Cell* 2013;**155**:1624–38
 60. Massudi H, Grant R, Braidy N, Guest J, Farnsworth B, Guillemin GJ. Age-associated changes in oxidative stress and NAD+ metabolism in human tissue. *PLoS One* 2012;**7**:e42357
 61. Mouchiroud L, Houtkooper RH, Moullan N, Katsyuba E, Ryu D, Canto C, Mottis A, Jo YS, Viswanathan M, Schoonjans K, Guarente L, Auwerx

- J. The NAD(+)/sirtuin pathway modulates longevity through activation of mitochondrial UPR and FOXO signaling. *Cell* 2013;**154**:430–41
62. Mouchiroud L, Houtkooper RH, Auwerx J. NAD(+) metabolism: a therapeutic target for age-related metabolic disease. *Crit Rev Biochem Mol Biol* 2013;**48**:397–408
63. Cerutti R, Pirinen E, Lamperti C, Marchet S, Sauve AA, Li W, Leoni V, Schon EA, Dantzer F, Auwerx J, Viscomi C, Zeviani M. NAD(+)-dependent activation of Sirt1 corrects the phenotype in a mouse model of mitochondrial disease. *Cell Metab* 2014;**19**:1042–9
64. Houtkooper RH, Auwerx J. Exploring the therapeutic space around NAD+. *J Cell Biol* 2012;**199**:205–9
65. Khan NA, Auranen M, Paetau I, Pirinen E, Euro L, Forsstrom S, Pasila L, Velagapudi V, Carroll CJ, Auwerx J, Suomalainen A. Effective treatment of mitochondrial myopathy by nicotinamide riboside, a vitamin B3. *EMBO Mol Med* 2014;**6**:721–31

(Received March 27, 2020, Accepted May 18, 2020)